crystals

Article

Dual Optical Frequency Comb Generation with Dual Cascaded Difference Frequency Generation

Yanli Yin [1], Kaiwu Wang [1], Gege Zhang [1], Zhongyang Li [1,*], Pibin Bing [1], Sheng Yuan [1], Anfu Zhu [1], Degang Xu [2] and Jianquan Yao [2]

1 College of Electrical Engineering, North China University of Water Resources and Electric Power, Zhengzhou 450045, China
2 College of Precision Instrument and Opto-Electronics Engineering, Institute of Laser and Opto-Electronics, Tianjin University, Tianjin 300072, China
* Correspondence: thzwave@163.com

Abstract: In this work, we propose a novel dual optical frequency comb (DOFC) generation scheme based on dual cascaded difference frequency generation (DCDFG). Feasible designs are introduced that enable the two sets of cascaded optical waves, initially generated by DCDFG in an aperiodically periodically poled lithium niobate (APPLN) crystal with a pump wave and two signal waves, then transferred to high-order Stokes waves by oscillations of cascaded Stokes waves and the optimization of phase mismatching of each-order DCDFG; finally, a DOFC was constructed. We demonstrate a high-performance DOFC with characteristics of high repetition frequency difference, tunable repetition frequency difference, high flatness, and a tunable spectral distribution range by providing a theoretical framework. We argue that the scheme proposed in this work is promising for achieving a high-quality DOFC.

Keywords: dual optical frequency comb; cascaded difference frequency generation; terahertz wave; aperiodically periodically poled lithium niobate

check for updates

Citation: Yin, Y.; Wang, K.; Zhang, G.; Li, Z.; Bing, P.; Yuan, S.; Zhu, A.; Xu, D.; Yao, J. Dual Optical Frequency Comb Generation with Dual Cascaded Difference Frequency Generation. *Crystals* **2022**, *12*, 1392. https://doi.org/10.3390/cryst12101392

Academic Editor: Yuri Kivshar

Received: 9 September 2022
Accepted: 28 September 2022
Published: 1 October 2022

1. Introduction

Optical frequency comb (OFC) represents a novel versatile tool with a wide range of applications, such as telecommunications [1], metrology [2], optical arbitrary waveform generation [3], microwave photonics [4], and spectroscopy [5]. Recently, dual optical frequency comb (DOFC) spectroscopy has been seen as a promising spectroscopic tool providing unprecedented frequency resolution, fast acquisition times, and high-sensitivity broadband spectroscopy [6]. OFC has an optical spectrum consisting of a series of discrete, same-frequency intervals and phase-locked frequency lines, while DOFC has two coherent OFCs with slightly differing repetition rates. OFC sources have been successfully demonstrated by nonlinear optical frequency conversion technology, such as difference frequency generation [7], optical parametric oscillator [8], and quantum-cascade laser optical frequency comb [9]. However, the generation of DOFC has not been reported by nonlinear optical frequency conversion technology. In this work, we propose a novel scheme for DOFC generation with dual cascaded difference frequency generation (DCDFG). The two sets of cascaded optical waves that are generated by DCDFG with an aperiodically periodically poled lithium niobate (APPLN) crystal are transferred to high-order Stokes waves by the oscillations of Stokes waves within a resonant cavity, and finally are transformed into DOFC. Compared with other DOFC generation schemes, the scheme proposed in this work has the following merit. DOFC is generated by DCDFG, and THz waves are generated simultaneously. The above process consists of second-order and third-order nonlinear frequency conversions. As the frequencies of THz waves lie in the vicinity of polariton resonances of MgO//$LiNbO_3$ crystal, the polariton resonances can induce giant nonlinearities, which are beneficial to the DOFC generation.

2. Theoretical Model

DCDFG, which is stimulated by three input lasers, ω_0, $\omega_{a,1}$, and $\omega_{b,1}$, produces two sets of cascaded optical waves $\omega_{a/b,m}$ (ω is frequency (cycles/second), m is an integer) and THz waves ($\omega_{T1/T2} = \omega_0 - \omega_{a/b,1}$), as shown in Figure 1a. $\omega_{a/b,m}$ is cascaded Stokes waves with $m > 1$ and cascaded anti-Stokes waves with $m \leq -1$, respectively. The generations of THz waves and cascaded optical waves relate to the pure parametric (second-order nonlinear process) and stimulated Raman scattering processes (third-order nonlinear process) [10]. The optical parametric oscillator (OPO) for cascaded Stokes waves is a widely used bow-tie resonant cavity [11], comprising four cavity mirrors C_1, C_2, C_3, and C_4. The concave mirrors C_1 and C_2 have a high transmittance for ω_0, $\omega_{a,1}$, $\omega_{b,1}$, and $\omega_{a/b,m}$ ($m \leq -1$). The concave mirrors C_1 and C_2 and the plane mirror C_3 have a high reflectivity for $\omega_{a/b,m}$ ($m > 1$), while the plane mirror C_4 is partial transmittance for $\omega_{a/b,m}$ ($m > 1$). The nonlinear gain medium is an APPLN crystal.

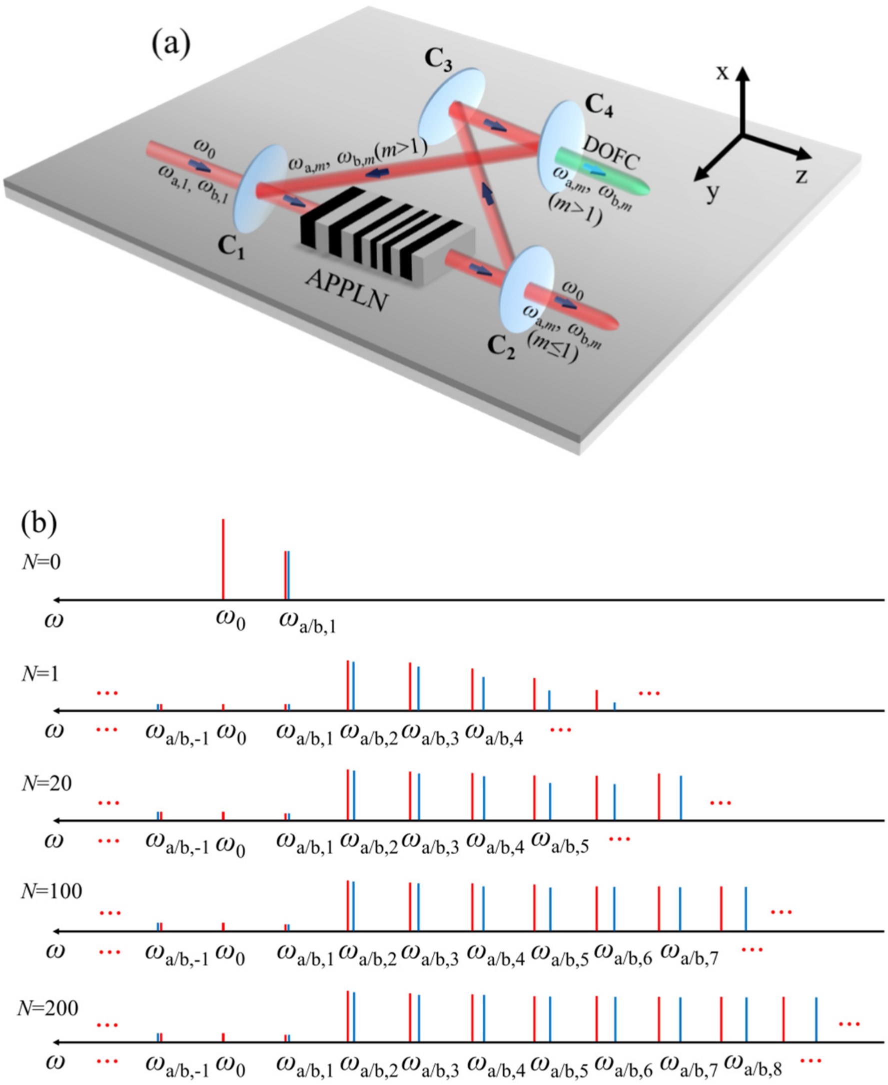

Figure 1. Schematic diagram of DOFC generation by DCDFG. ω_0 and $\omega_{a,1}$ generate a set of cascaded optical waves $\omega_{a,m}$ and THz wave ω_{T1}, respectively. ω_0 and $\omega_{b,1}$ generate a set of cascaded optical waves $\omega_{b,m}$ and THz wave ω_{T2}, respectively. (**a**) Schematic diagram of a bow-tie resonant cavity for cascaded optical Stokes waves; C_1, C_2, C_3, and C_4 are resonant cavity mirrors, and APPLN is a nonlinear optical crystal. (**b**) The interaction of the two sets of $\omega_{a,1}$ and $\omega_{b,m}$ generating DOFC; N is the number of oscillations of cascaded optical waves $\omega_{a/b,m}$.

The three input lasers ω_0, $\omega_{a,1}$, and $\omega_{b,1}$ stimulate the APPLN crystal and generate several spectral lines for the first oscillation of cascaded Stokes waves N = 1 (N is the oscillation number, which means N times round trip of the cascaded Stokes waves in the resonator). As N increases from 1 to 20 and 100, the spectral lines increase rapidly in high-order Stokes region, and the intensities of the spectral lines are gradually identical. As N increases from 100 to 200, the number and the intensity of spectral lines become invariable, resulting in the formation of DOFC. The coupled wave equations of DCDFG within OPO are derived as follows [12,13]:

$$\frac{dE_{\mathrm{T1}}}{dz} = -\frac{\alpha_{\mathrm{T1}}}{2}E_{\mathrm{T1}} + j\frac{\Omega_{\mathrm{T1}}d_{eff}}{cn_{\mathrm{T1}}}\sum_{m=-\infty}^{m=+\infty} E_{\mathrm{a},m}E^*_{\mathrm{a},m+1}e^{j\Delta k_{\mathrm{a},m}z} \tag{1}$$

$$\frac{dE_{\mathrm{T2}}}{dz} = -\frac{\alpha_{\mathrm{T2}}}{2}E_{\mathrm{T2}} + j\frac{\Omega_{\mathrm{T2}}d_{eff}}{cn_{\mathrm{T2}}}\sum_{m=-\infty}^{m=+\infty} E_{\mathrm{b},m}E^*_{\mathrm{b},m+1}e^{j\Delta k_{\mathrm{b},m}z} \tag{2}$$

$$\frac{dE_{\mathrm{a},m}}{dz} = -\frac{\alpha_{\mathrm{a},m}}{2}E_{\mathrm{a},m} + \sum_{N=1}^{N} R_1^{N-1}R_2^{N-1}R_3^{N-1}(1-R_4)^{N-1}\left(j\frac{\Omega_{\mathrm{a},m}d_{eff}}{cn_{\mathrm{a},m}}\left[E_{\mathrm{a},m-1}E^*_{\mathrm{T1}}e^{j\Delta k_{\mathrm{a},m-1}z} + E_{\mathrm{a},m+1}E_{\mathrm{T1}}e^{-j\Delta k_{\mathrm{a},m}z}\right]\right) \tag{3}$$

$$\frac{dE_{\mathrm{b},m}}{dz} = -\frac{\alpha_{\mathrm{b},m}}{2}E_{\mathrm{b},m} + \sum_{N=1}^{N} R_1^{N-1}R_2^{N-1}R_3^{N-1}(1-R_4)^{N-1}\left(j\frac{\Omega_{\mathrm{b},m}d_{eff}}{cn_{\mathrm{b},m}}\left[E_{\mathrm{b},m-1}E^*_{\mathrm{T2}}e^{j\Delta k_{\mathrm{b},m-1}z} + E_{\mathrm{b},m+1}E_{\mathrm{T2}}e^{-j\Delta k_{\mathrm{b},m}z}\right]\right) \tag{4}$$

$$\Delta k_{\mathrm{a},m} = k_{\mathrm{a},m} - k_{\mathrm{a},m+1} - k_{\mathrm{T1}} + k_{\Lambda} \tag{5}$$

$$\Delta k_{\mathrm{b},m} = k_{\mathrm{b},m} - k_{\mathrm{b},m+1} - k_{\mathrm{T2}} + k_{\Lambda} \tag{6}$$

$$I = \frac{1}{2}nc\varepsilon_0|E|^2 \tag{7}$$

where the subscript m, T1, and T2 represent the mth-order cascaded optical wave, the THz wave generated by ω_0 and $\omega_{a,1}$, and the THz wave generated by ω_0 and $\omega_{b,1}$, respectively; Ω is angular frequency (radians/second); E is the electric field strength; α is the absorption coefficient; and n is the refractive index. R_1, R_2, R_3, and R_4 are the reflectance of C_1, C_2, C_3, and C_4 for cascaded Stokes waves, respectively. k is the wave vector, Δk represents the phase mismatch, and d_{eff} is the nonlinear coefficient involving both electronic and vibrational contributions of the APPLN crystal [14]. Λ represents the poling period of the APPLN crystal, c is the vacuum speed of light, ε_0 represents the vacuum permittivity, and I represents the intensity. In Equation (1), the first item indicates absorption of THz wave, and the second item indicates the sum of THz wave intensities generated by the interaction of cascaded optical waves $\omega_{a,m}$ and $\omega_{a,m+1}$. In Equation (2), the first item indicates absorption of THz wave and the second item indicates the sum of THz wave intensities generated by the interaction of cascaded optical waves $\omega_{b,m}$ and $\omega_{b,m+1}$. In Equation (3), the first item indicates absorption of the cascaded optical waves, and the second item indicates the generation of $\omega_{a,m}$ by the interaction between $\omega_{a,m-1}$ and ω_{T1}, and the third term describes the generation of $\omega_{a,m}$ by the interaction between $\omega_{a,m+1}$ and ω_{T1}. In Equation (4), the first item indicates absorption of the cascaded optical waves, and the second item indicates the generation of $\omega_{b,m}$ by the interaction between $\omega_{b,m-1}$ and ω_{T2}, and the third term describes the generation of $\omega_{b,m}$ by the interaction between $\omega_{b,m+1}$ and ω_{T2}.

3. Calculations

The frequencies of ω_0, $\omega_{a,1}$, and $\omega_{b,1}$ were 281.9, 281.8, and 281.7998 THz, respectively, corresponding the THz wave frequencies ω_{T1} and ω_{T2} of 0.1 THz and 0.1002 THz, respectively. The frequency 281.9 THz corresponded to the wavelength of 1.0642 µm, the wavelength of a Nd/YAG laser. The nonlinear coefficient of APPLN crystal at 281.9 THz was 336 pm/V [10]. The intensities of the three pulsed input lasers ω_0, $\omega_{a,1}$, and $\omega_{b,1}$ were 100, 1, and 1 MW/cm^2, respectively. The Sellmeier equations for cascaded optical waves and THz waves at room temperature were from references [15] and [16], respectively. All the reflectivities of R_1, R_2, and R_3 were 0.9999, and the reflectivity of R_4 was 0.98.

In the process of DOFC generation, the evolution of cascaded optical waves was determined by phase mismatches of DCDFG $\Delta k_{a/b,m}$. The phase mismatches $\Delta k_{a/b,m}$ were set to be the minimum value from the first-order cascaded difference frequency generation (CDFG) to the mth-order($m \gg 1$) CDFG one order by one order, transferring the photons from low-order Stokes waves to high-order Stokes waves. The above setting was achieved by Equation (8):

$$\Lambda = c \times \begin{pmatrix} -n_{\frac{m\times z}{L}} \times (\omega_0 - \omega_{TA} \times (\frac{m\times z}{L})) + n_{1+\frac{m\times z}{L}} \times \\ ((\omega_0 - \omega_{TA} \times (\frac{m\times z}{L})) - \omega_{TA}) + \omega_{TA} \times n_{TA} \end{pmatrix}^{-1} \quad (8)$$

where $\omega_{T1} < \omega_{TA} < \omega_{T2}$, $0 < z \leq L$. L is the length of APPLN crystal, and n_{TA} is the refractive index of ω_{TA}. ω_{TA} of 0.10015 THz in the following calculations ensured that the photon transfer in two CDFG processes from ω_0 and $\omega_{a,1}$ to $\omega_{a,m}$ and from ω_0 and $\omega_{b,1}$ to $\omega_{b,m}$ were balanced.

The evolution of DOFC versus oscillation number N is calculated according to Equations (1)–(8), as shown in Figure 2. From the figure, it can be seen that when $N < 10$, the cascaded Stokes waves transferred to high-order Stokes waves rapidly, and the intensities of the cascaded Stokes waves varied drastically. When $10 < N < 50$, the cascaded Stokes waves transferred to higher-order Stokes waves rapidly, and the intensities of the cascaded Stokes waves changed moderately. When $50 < N < 200$, the transformation of cascaded Stokes waves to higher-order Stokes waves was slow, and the intensities of the cascaded Stokes waves tended to be stable. When $N = 200$, the cascaded Stokes waves were converted to a high-quality DOFC, as shown in Figure 2b,c. The repetition frequency difference Δf_{rep} of the DOFC was 200 MHz, the spectrum range of the DOFC within 1 dB flatness was 259.3 THz–275.2 THz, and the number of the comb line was 160.

From Equation (8), we find that cascading order m can influence phase mismatches $\Delta k_{a/b,m}$. Figure 3a shows the spectral distribution of DOFC with different cascading order m, and the dashed boxes in Figure 3a corresponding to DOFC were enlarged, shown in Figure 3b. The spectral range of DOFC within 1 dB flatness was 262.9–272 THz for $m = 50$. With the cascading order m increasing from 50 to 100, 150, 200, and 250, DOFC spectral range within 1 dB flatness firstly expanded and then reduced. The largest spectral range was 259.3–275.2 THz for $m = 200$. With the cascading order m increasing from 50 to 100, 150, 200, and 250, the comb line number of the DOFC within 1 dB flatness increased from 92 to 102, 121, and 160, and then decreased to 100. The DOFC spectrum range of 1086.96–1156.96 nm within 1 dB flatness can be achieved with different cascading order m.

Equations (1) and (2) show that phase mismatches $\Delta k_{a/b,m}$ affected the interaction of cascaded Stokes waves. The interaction length of the mth-order CDFG was ΔL_m, and $\Delta L_m = L/m$. By changing the crystal length L and keeping cascading order m constant, the variable ΔL_m changed the transfer speed of the cascaded Stokes waves to high-order Stokes waves. Figure 4a shows the spectral distribution of DOFC with different crystal lengths L. The DOFC spectrum range of 271–280.1 THz was extremely narrow for $L_1 = 4$ cm. As the crystal length L increased from 4 cm to 4.5 cm, 5 cm, 5.5 cm, and 6 cm, the DOFC spectral range gradually increased and rapidly moved to the long-wavelength range. The DOFC spectrum range was 259.3–275.2 THz for $L = 6$ cm. As the crystal length increased from 4 cm to 4.5 cm, 5 cm, 5.5 cm, and 6 cm, the comb line number of DOFC within 1 dB flatness increased from 92 to 111, 124, 135, and 160. With the above five crystal lengths, the DOFC spectrum range of 1071.05–1156.96 nm within 1 dB flatness can be achieved. The reason for the above phenomenon is that when the ΔL_m was short, the photon transfer from the mth order Stokes wave to the $(m + 1)$th order Stokes was extremely insufficient, resulting in the narrow DOFC spectrum range. As discussed above, the number of comb lines, the amount of flatness, and the spectral distribution range of DOFC can be tuned by adjusting the crystal length. From Figures 3 and 4, we find that the wide tuning of DOFC spectrum range can be realized by changing the crystal length L, while the precise tuning of the DOFC spectrum range can be achieved by changing the cascading order m.

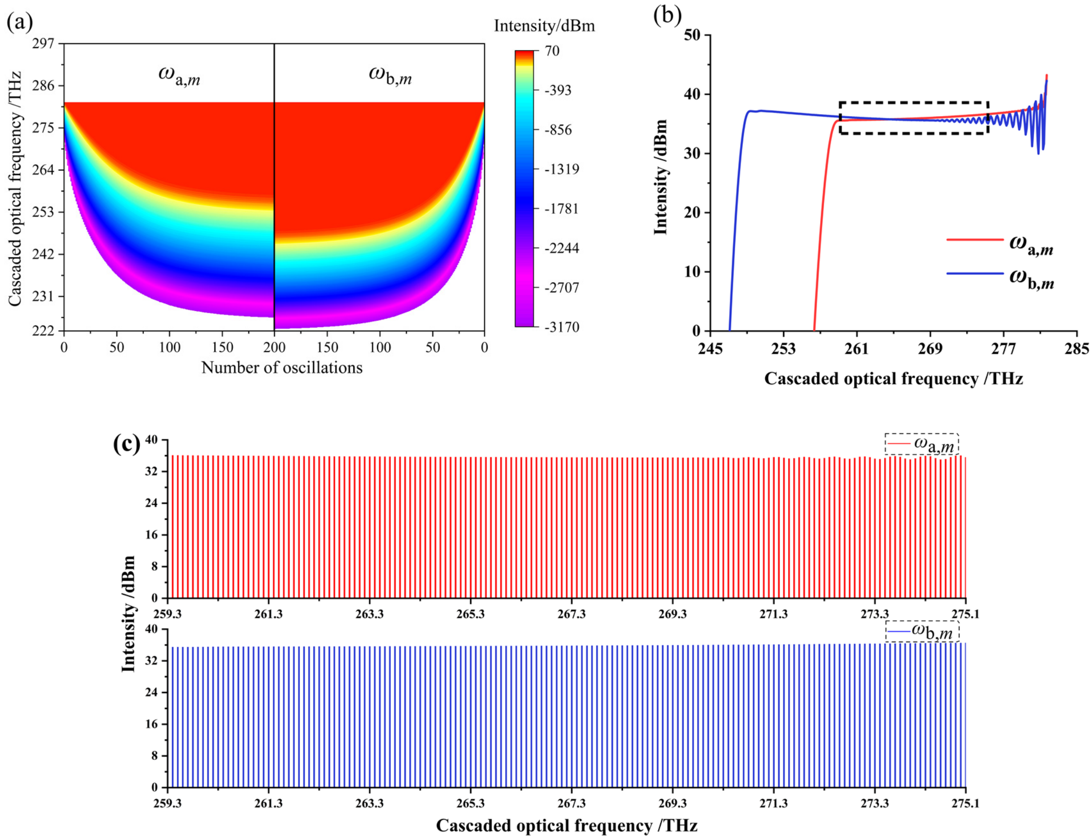

Figure 2. Evolution of DOFC generated by DCDFG within the OPO. m = 200, L = 6 cm, I_0 = 100 MW/cm^2, I_1 = 1 MW/cm^2, I_2 = 1 MW/cm^2. (**a**) Evolution of $\omega_{a,m}$ and $\omega_{b,m}$ with oscillation number N. (**b**) Spectral distribution of $\omega_{a,m}$ and $\omega_{b,m}$ with N = 200; the range covered by the dashed box was DOFC within 1 dB flatness. (**c**) Enlargement of the range covered by the dashed box in (**b**).

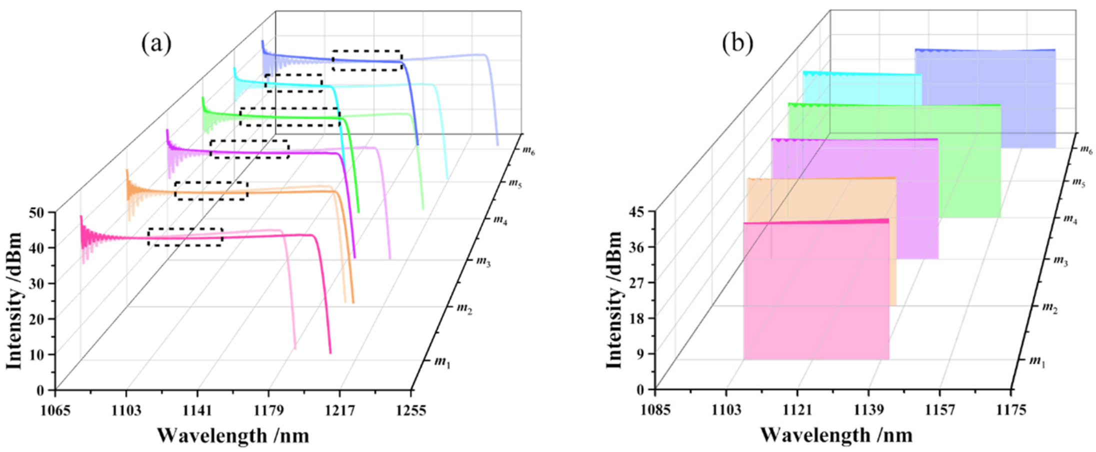

Figure 3. Spectral distribution of DOFC with different cascading order m, cascading order m_1 = 50, m_2 = 100, m_3 = 150, m_4 = 200, m_5 = 250, L = 6 cm, N = 200, I_0 = 100 MW/cm^2, I_1 = 1 MW/cm^2, I_2 = 1 MW/cm^2. (**a**) Spectral distribution of DOFC with different cascading order m; the range covered by the dashed box was DOFC within 1 dB flatness. (**b**) Enlargement of the dashed box in (**a**).

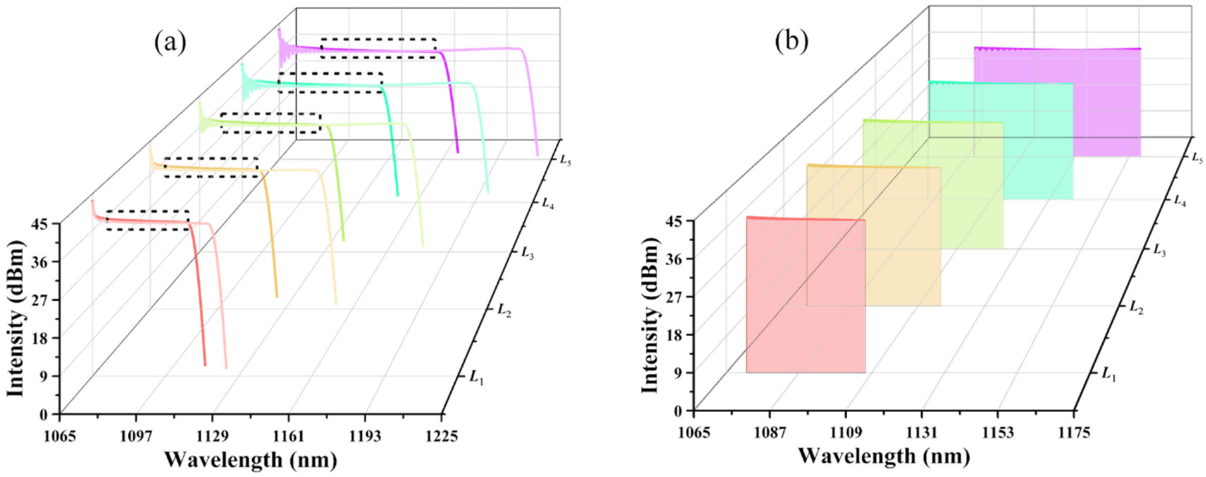

Figure 4. Spectral distribution of DOFC with different crystal lengths L. Crystal length L_1 = 4.0 cm, L_2 = 4.5 cm, L_3 = 5.0 cm, L_4 = 5.5 cm, L_5 = 6.0 cm, m = 200, N = 200, I_0 = 100 MW/cm^2, I_1 = 1 MW/cm^2, I_2 = 1 MW/cm^2. (a) Spectral distribution of DOFC with different crystal lengths L; the range covered by the dashed box was DOFC within 1 dB flatness. (**b**) Enlargement of the dashed box in (**a**).

DOFC with different repetition frequency differences Δf_{rep} can be obtained by changing the frequency of $\omega_{b,1}$, while the two frequencies ω_0 and $\omega_{a,1}$ are constant. Figure 5 illustrates the DOFC formation process for Δf_{rep} = 300 and 400 MH. It can be seen from the figure that the cascaded Stokes waves firstly rapidly and then slowly transferred to higher-order Stokes waves as the oscillation number N increased. A stable DOFC was formed when N = 200. Comparing Figure 5 with Figure 2, when the repetition frequency difference Δf_{rep} increased from 200 MHz to 300 MHz and 400 MHz, the spectral distribution range of DOFC was reduced from 259.3–280.1 THz to 259.2–268.6 THz and 259.9–266.3 THz, respectively. The reason was that as Δf_{rep} increased, the phase mismatch $\Delta k_{a/b,m}$ of the mth order CDFG was enlarged, resulting in a slow photon transfer from the mth order Stokes wave to the $(m + 1)$th order Stokes wave.

The high-performance DOFC had characteristics of high repetition frequency difference, tunable repetition frequency difference, high flatness, and tunable spectral distribution range attributes of the repeated and continuous frequency conversions from ω_0 to high-order Stokes waves. The repeated frequency conversions were accomplished by oscillations of Stoke waves in a resonant cavity. The continuous frequency conversions were accomplished by optimized DCDFG with Equation (8). Compared with APPLN with a quasi-phase matching configuration in this work, the cascading with cherenkov cut MgO/LiNbO3 crystal was difficult to realize because noncollinear phase-matching restricts the interaction volume of mixing waves.

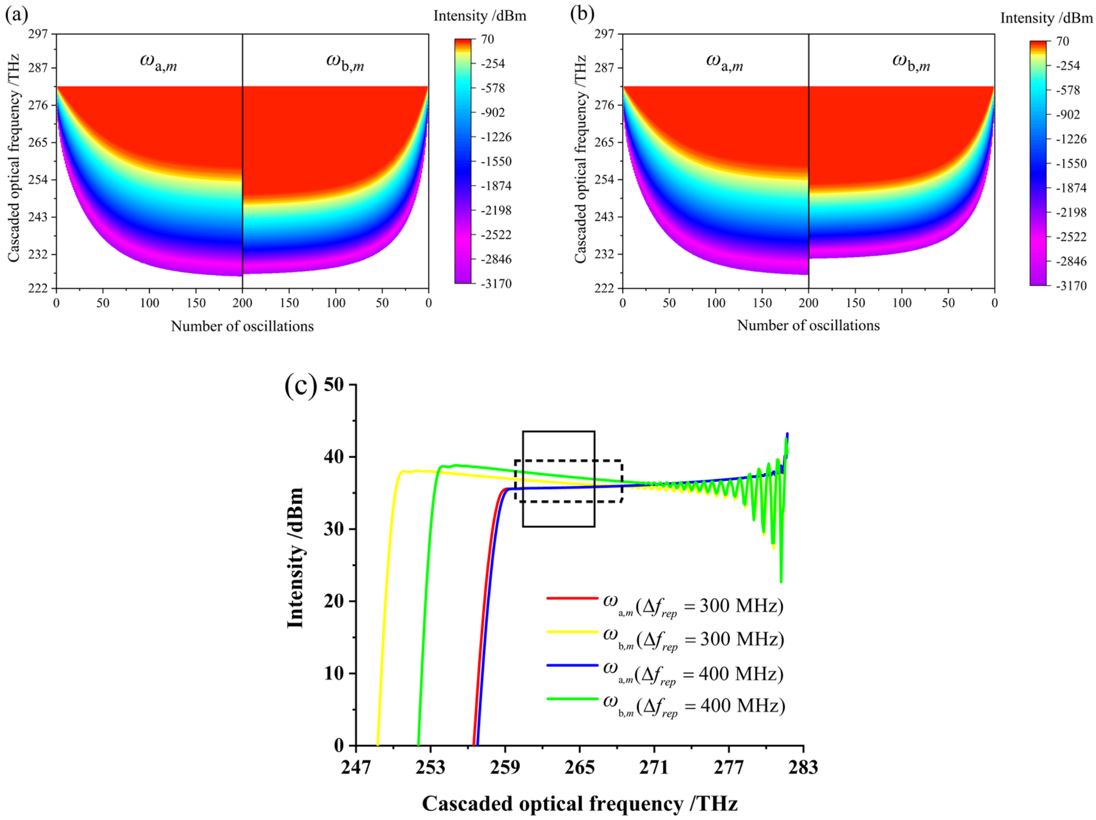

Figure 5. Evolution process of DOFC generated by DCDFG within the OPO. m = 200, L = 6 cm, I_0 = 100 MW/cm^2, I_1 = 1 MW/cm^2, I_2 = 1 MW/cm^2; ω_0 and $\omega_{a,1}$ are 281.9 THz and 281.8 THz, respectively. (**a**) Evolution of DOFC generated by DCDFG within the OPO with oscillation number N; $\omega_{b,1}$ = 281.7997 THz, Δf_{rep} = 300 MHz. (**b**) Evolution of DOFC generated by DCDFG within the OPO with oscillation number N; $\omega_{b,1}$ = 281.7996 THz, Δf_{rep} = 400 MHz. (**c**) Spectral distribution of DOFC with N = 200; the dashed box indicates Δf_{rep} = 300 MHz within 1 dB flatness, and the solid box indicates Δf_{rep} = 400 MHz within 1 dB flatness.

4. Conclusions

In this work, a novel DOFC generation scheme based on DCDFG combined with OPO is proposed. The simulation results show that by increasing the APPLN crystal length, the DOFC spectrum range was greatly broadened and the DOFC spectral distribution was rapidly red-shifted, and simultaneously the comb line number of DOFC within 1 dB flatness was greatly increased. By increasing the cascading order of CDFG, the DOFC spectral distribution range was firstly expanded and then reduced, and simultaneously the comb line number of DOFC within 1 dB flatness firstly increased and then was reduced. By changing the frequency difference among the three input lasers, the repetition frequency difference of DOFC can be tuned and the DOFC spectral range is effectively expanded. The novel scheme proposed in this work paves the way for high-performance DOFC source.

Author Contributions: Conceptualization, Y.Y. and Z.L.; methodology, K.W. and G.Z.; software, K.W. and G.Z.; validation, K.W. and G.Z.; data curation, K.W. and G.Z.; writing—original draft preparation, K.W. and G.Z.; writing—review and editing, Y.Y. and Z.L.; supervision, P.B., S.Y., A.Z., D.X., and J.Y. All authors have read and agreed to the published version of the manuscript.

Funding: This research was funded by the National Natural Science Foundation of China (grant nos. 61735010, 31671580, 61601183), the Natural Science Foundation of Henan Province (grant no. 162300410190), and the Key Scientific Research Project of Henan Universities (grant no. 19A510004).

Institutional Review Board Statement: Not applicable.

Informed Consent Statement: Not applicable.

Data Availability Statement: Data underlying the results presented in this paper are not publicly available at the time of publication, which may be obtained from the authors upon reasonable request.

Conflicts of Interest: The authors declare no conflict of interest.

References

1. Delfyett, P.J.; Gee, S.; Choi, M.-T.; Izadpanah, H.; Lee, W.; Ozharar, S.; Quinlan, F.; Yilmaz, T. Optical frequency combs from semiconductor lasers and applications in ultrawideband signal processing and communications. *J. Lightwave Technol.* **2006**, *24*, 2701–2719. [CrossRef]
2. Pupeza, I.; Zhang, C.K.; Högner, M.; Ye, J. Extreme-ultraviolet frequency combs for precision metrology and attosecond science. *Nat. Photonics* **2021**, *15*, 175–186. [CrossRef]
3. Bosworth, B.T.; Jungwirth, N.R.; Smith, K.; Cheron, J.; Quinlan, F.; Woodson, M.; Morgan, J.; Beling, A.; Williams, D.; Orloff, N.D.; et al. Electro-optically derived millimeter-wave sources with phase and amplitude control. *Appl. Phys. Lett.* **2021**, *119*, 151106. [CrossRef]
4. Chen, B.; Fan, Y.Y.; Liu, T.; Gao, Y.S.; Xue, X.Q.; Liu, Y. Broadband photonic RF channelizer with 66 channels based on acousto-optic frequency shifter. *Opt. Eng.* **2021**, *60*, 126102. [CrossRef]
5. Chandran, S.; Ruth, A.A.; Martin, E.P.; Alexander, J.K.; Peters, F.H.; Anandarajah, P.M. Off-Axis Cavity-Enhanced Absorption Spectroscopy of $^{14}NH_3$ in Air Using a Gain-Switched Frequency Comb at 1.514 µm. *Sensors* **2019**, *19*, 5217. [CrossRef] [PubMed]
6. Coddington, I.; Newbury, N.; Swann, W. Dual-comb spectroscopy. *Optica* **2016**, *3*, 414–426. [CrossRef] [PubMed]
7. Cruz, F.C.; Maser, D.L.; Johnson, T.; Ycas, G.; Klose, A.; Giorgetta, F.R.; Coddington, I.; Diddams, S.A. Mid-infrared optical frequency combs based on difference frequency generation for molecular spectroscopy. *Opt. Express* **2015**, *23*, 26814–26824. [CrossRef] [PubMed]
8. Lee, K.F.; Granzow, N.; Schmidt, M.A.; Chang, W.; Wang, L.; Coulombier, Q.; Troles, J.; Leindecker, N.; Vodopyanov, K.L.; Schunemann, P.G.; et al. Midinfrared frequency combs from coherent supercontinuum in chalcogenide and optical parametric oscillation. *Opt. Lett.* **2014**, *39*, 2056–2059. [CrossRef] [PubMed]
9. Hugi, A.; Villares, G.; Blaser, S.; Liu, H.C.; Faist, J. Mid-infrared frequency comb based on a quantum cascade laser. *Nature* **2012**, *492*, 229–233. [CrossRef] [PubMed]
10. Ravi, K.; Schimpf, D.N.; Kärtner, F.X. Pulse sequences for efficient multi-cycle terahertz generation in periodically poled lithium niobate. *Opt. Express* **2016**, *24*, 25582–25607. [CrossRef] [PubMed]
11. Kiessling, J.; Sowade, R.; Breunig, I.; Dierolf, V. Cascaded optical parametric oscillations generating tunable terahertz waves in periodically poled lithium niobate crystals. *Opt. Express* **2009**, *17*, 87–91. [CrossRef]
12. Li, Z.Y.; Yan, Q.Z.; Liu, P.X.; Jiao, B.Z.; Zhang, G.G.; Chen, Z.L.; Bing, P.B.; Yuan, S.; Zhng, K.; Yao, J.Q. Terahertz wave generation by repeated and continuous frequency conversions from pump wave to high-order Stokes waves. *Chin. Phys. B* **2022**, *31*, 0742909.
13. Liu, P.X.; Qi, F.; Pang, Z.B.; Li, W.F.; Wang, Y.L.; Liu, Z.Y.; Meng, D.L. Cascaded difference frequency generation in organic crystal 4′-dimethylamino-N-methyl-4-stilbazolium tosylate. *Opt. Lett.* **2019**, *44*, 4965–4968. [CrossRef]
14. Mayer, A.; Keilmann, F. Far-infrared nonlinear optics. I. $\chi^{(2)}$ near ionic resonance. *Phys. Rev. B* **1986**, *33*, 6954–6961. [CrossRef]
15. Jundt, D.H. Temperature-dependent Sellmeier equation for the index of refraction, n_e, in congruent lithium niobate. *Opt. Lett.* **1997**, *22*, 1553–1555. [CrossRef]
16. Pálfalvi, L.; Hebling, J.; Kuhl, J.; Pter, Á.; Polgár, K. Temperature dependence of the absorption and refraction of Mg-doped congruent and stoichiometric $LiNbO_3$ in the THz range. *J. Appl. Phys.* **2005**, *97*, 123505. [CrossRef]